THERMO-MECHANICAL INVESTIGATIONS DURING FRICTION STIR SPOT WELDING (FSSW) OF AA6082-T6


S.U. Khosa


T. Weinberger


N. Enzinger

ABSTRACT

Friction Stir Spot Welding (FSSW) is a variant of the Friction Stir Welding (FSW) process and has been successfully used in industrial applications. During the FSSW process, thermal inputs due to friction and deformation are commenced simultaneously, as the non-consumable rotating tool plunges into the workpiece to be welded. Various assumptions and hypotheses for mechanisms of heat generation and material deformation during FSW/FSSW process are reported, but a consensus is still to be reached. The joining quality is mainly dependent upon the material flow in this solid state joining technique. The material flow and deformations in the near and far fields of the weld are directly affected by the temperature-sensitive mechanical properties. Therefore, a comprehension of thermo-mechanical responses are of high importance from the viewpoints of parameter optimization and understanding of the mechanisms . The FSSW process is experimentally and theoretically studied to address these issues of the mechanism of heat generation and coupled thermo-mechanical response of the workpiece, as well as the effects of tool rotation and plunge speeds. For theoretical studies, a 3-dimensional, physical-based FEM (Finite Element Method) model is developed using commercial code. For heat generation, friction and deformation-based formulations are used. For material responses, thermal and strain rate-sensitive, elastic-plastic data are employed by a constitutive Johnson Cook material model and thermo-mechanical behaviour is analyzed with respect to experimental observations. To cope with high calculation time and distortion of the mesh, built-in features of the code, mass scaling, ALE (Arbitrary Lagrangian Eulerian) and mesh re-mapping were used. As a result of this work, a basic platform in the form of a physical-based, coupled, thermo-mechanical model is developed. With the help of this model, effects of process parameters on the temperature – displacement behaviour of the workpiece are studied. The role of interaction conditions at the tool-workpiece interface is emphasized and a simplified conceptual mechanism for effects of process variables on the physical phenomena is presented.

IIW-Thesaurus keywords: *Computation; Deformation; Finite element analysis; Friction stir welding; Heat; Reference lists.*

M.Sc.Saleem U. KHOSA (saleem.khosa@student.tugraz.at), Research Associate/Ph.D. Student, Dipl.-Ing. Thomas WEINBERGER (thomas.weinberger@tugraz.at) and Dipl.-Ing., Dr. techn. Norbert ENZINGER (norbert.enzinger@tugraz.at) are all with Institute for Materials Science and Welding (IWS), Graz University of Technology, Graz (Austria). They are all associated with JOIN – Network of Excellence for Joining, Austria.

Doc. IIW-1968-08 (ex-doc. IX-2284r1-08), recommended for publication by Commission IX “Behaviour of metals subjected to welding.”

1 INTRODUCTION

Friction Stir Welding (FSW) and its variant, Friction Stir Spot Welding (FSSW), are relatively new, solid state joining approaches which have exhibited remarkable prospects in various industrial sectors (e.g. transport, aerospace, etc.) [1-3]. The potential of FSSW among the spot joining processes is increasing. For example, Mazda reported a more than 90 % reduction in energy consumption, relative to the conventional spot joining technique, when FSSW was used for one of its automobile models [4]. This scenario raises the need for a

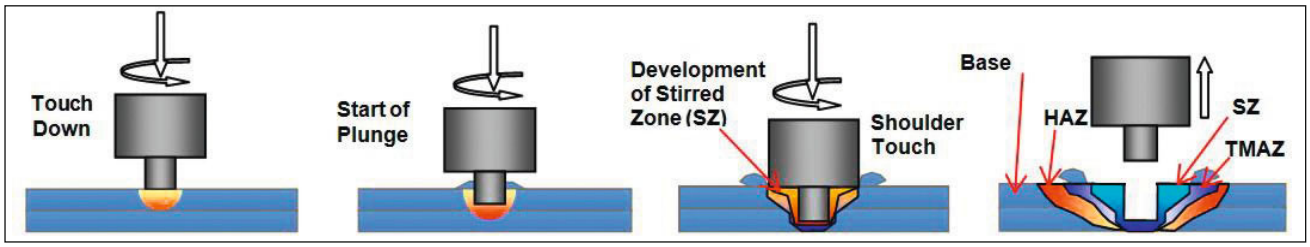

a) Touchdown of the pin **b) Start of pin penetration to commence the plunge** **c) Plunge ends by the shoulder touch with or without dwell time** **d) Retraction of the tool**

Figure 1 – Schematic of FSSW process [6]

deeper understanding of the mechanisms involved in this process.

1.1 Basics of the process

Apart from touch-down and retraction, the whole FSW process may be divided into plunge, dwell and traverse welding [2, 5]. Thermal and material flow fields developed during the plunge and dwell stages are translated along the weld line during the traverse motion of the tool.

During the FSSW process, the traverse motion of the tool is not carried out and hence only a spot weld is achieved. As schematically shown in Figure 1 [6], stages of the FSSW process may be described as: a) touchdown of the pin of the tool, b) plunge initiation, c) shoulder touchdown, with or without some dwell time, and d) retraction of the tool.

Based on microstructural characterization of grains and precipitates, a typical weld zone in an FSSW joint contains a Stirred Zone (SZ), a Thermo-Mechanically Affected Zone (TMAZ) and a Heat-Affected Zone (HAZ). These zones, along with the Base Material (BM) region, are marked on the macrograph in Figure 2.

Intense plastic deformation and frictional heating during FSW/FSSW result in the generation of a re-crystallized, fine-grained microstructure within the stirred zone (SZ) [2]. During the welding process, the SZ is plasticized or softened to such a degree that it may be assumed to be pseudo-fluid. Numerous theoretical flow-visualization studies have solved the problem with fluid dynamics formulations e.g. [7, 8].

Unique to the FSW/FSSW process is the creation of a transition zone between the base material (BM) and stirred zone (SZ) – namely the Thermo-Mechanically Affected Zone (TMAZ) [2]. In the TMAZ both the temperature and deformations effects of the process are experienced, but to a lesser extent than that in the SZ. Hence it is characterized by highly deformed structure but without re-crystallized fine-grained structure which is typical to SZ.

The zone beyond the TMAZ, where no major effects of deformation rather only temperature effects are experienced, also shows microstructural changes relative to the base material (BM). This zone is called the Heat-Affected Zone (HAZ). It may be characterized as the zone experiencing temperature rise above 250 °C for heat treatable aluminum alloys [9].

1.2 Motivation

Above mentioned zones are produced due to thermo-mechanical loads generated during the process and have significant effect on post-weld mechanical properties. Therefore research into the generation of these loads and the workpiece response are quite significant.

Due to inherent simplicity of FSSW relative to the FSW process, as complexities in heat generation and material flow mechanisms during traverse motion of the tool are not present, it may provide a basic platform for investigations of the afore mentioned mechanisms.

Because of limitation during experimental studies for direct measurements of thermal and flow fields within the weld zone for the FSW related processes, theoretical studies for estimation of these have been extensively performed. Most of these theoretical studies do not cover the plunge phase, for simplification. However

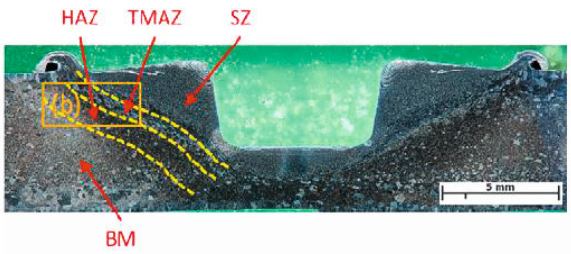

a) Different zones in a typical FSSW joint: SZ – Stirred Zone, TMAZ – Thermo-Mechanically Affected Zone, HAZ – Heat-Affected Zone and BM – Base Material

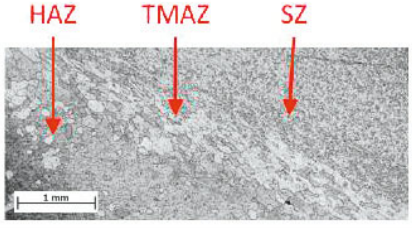

b) Details of characteristic microstructural appearance for SZ, TMAZ and HAZ

Figure 2

for the FSSW studies this is the main process phase and hence it cannot be neglected.

Fewer studies are reported in the literature for the FSSW process than for the FSW one and theoretical studies are even scarcer. The major challenge for theoretical study of the FSSW process is to investigate, the relatively short but highly transient plunge phase. During this phase transition of material from rigid solid to low strength viscous behaviour and the distortion of the mesh pose the major challenges. Moreover, understanding of the mechanisms of the generation of coupled thermal and mechanical loads during the process requires a physical-based model. For that, the definition of tool – workpiece interfacial conditions becomes very crucial. From tool design and the FSW/FSSW applications for a high-strength materials point of view as well, a detailed study of this phase of the process is very important.

Experimental studies to investigate the FSSW related issues, in reviewed literature, mainly focus on

a) feasibility of the process for different materials or combination of materials [10-12] and

b) effect of process parameters on different weld properties and their optimization [12-14].

Only few studies e.g. [15] investigated any process mechanism issues. These issues are generally addressed by theoretical investigations of the process e.g. [3, 5, 16, 17].

Reported theoretical studies for FSSW and the plunge phase of the FSW process employed three-dimensional numerical models based upon Computational Fluid Dynamics (CFD) [16] and solid mechanics [17] approaches. Both of these studies investigated small plunge depths considering only the first part of the plunge phase, neglecting higher deformation, increased heat input and shoulder touchdown [5]. Lately, 3-D, transient and thermo-mechanical coupled models have been published [3, 5] with the similar approach as the one presented in this study. The approach employed in [3] is based upon elastic-plastic material model and in [5] the Johnson-Cook (JC) material law is employed. However the relationship between the process variables and the physical phenomena has not been discussed in these studies.

To address these challenges and open points, a thermo-mechanical, fully coupled, 3-dimensional transient model is developed in FEM (Finite Element Methods) explicit formulations.

2 SIMPLIFIED CONCEPTUAL MECHANISM OF PROCESS

A simplified conceptual mechanism for the relationship between the process variables and the physical phenomena happening during the FSSW process may be described in the flow chart shown in Figure 3. In this

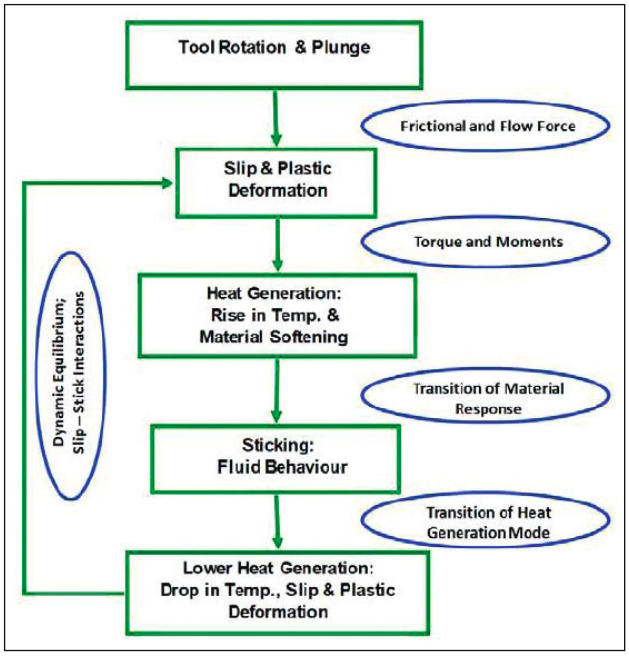

Figure 3 – Flow chart for simplified conceptual description of FSSW process

flow chart rectangles represent processes and ovals are resulting physical phenomena.

As a result of the experimental and theoretical studies presented in this paper, an attempt has been made to establish the relevance of this conceptual mechanism with the thermo-mechanics of the FSSW process.

It may be assumed that:

– As the rotating tool commences the touchdown on the top surface of the workpiece, its rotational and vertical motion is resisted by the interfacial friction (dynamic) and (yield/flow) strength of the base material.

– After the touchdown, the tool continues to plunge into the workpiece by having a tangential slipping over the surface contour of the workpiece, which is produced by the vertical motion of the tool. Depending upon the resisting forces and the tool geometry, torques and moments are experienced. These torque and moments lead to thermal inputs (at the interface and within the workpiece material).

– The heat generation, due to frictional force and dissipated deformational energy, raises the temperature in the vicinity of the tool – workpiece interface. Material softening due to drop in flow stress at higher temperature occurs.

– Another important factor concerning the drop in yield/flow strength of the base material may be the dissolution of the strengthening second phase particles for the age hardenable or heat treatable alloys apart from stress relieving due to elevated temperatures.

– The transition in material response (from rigid solid to softened or reduced strength visco-plastic response) may start the sticking interfacial conditions. One may imagine that interaction mode at the interface shifts from full slipping conditions to partial slip and stick conditions, with major fraction of slipping, i.e. co-existence of slip and stick interfacial conditions [18,

19]. This may also lead to changes in the torques and moments of the system.

– If the softened zone within workpiece, keeps on establishing itself depending upon its thermal behaviour (conductivity, capacity etc), the fraction of sticking mode may also increase.

– Assuming that major heat input is caused by friction [2-5, 20], the total heat input may be expected to drop down a bit, as increase in the fraction of sticking mode at the interface would lower the frictional heat input.

– Though it may be argued that during sticking conditions, the fraction of heat input due to dissipation of deformational energy may increase and balance the dropped fraction of frictional heat input.

– However, since the sticking conditions may only prevail when workpiece material has been softened considerably, therefore, overall energy input requirements of the system would be reduced. This assumption may be supported by the experimentally observed effect of drop in torques of the system.

– With this slight drop in total heat input, the fraction of slip mode for interfacial interaction between tool and workpiece may rise back.

– In the light of above discussion, it may be assumed, from a conceptual mechanism stand point, that after the initial transient period these conditions may develop a kind of dynamic equilibrium, if the process and system parameters are not changed.

– Thus for a given set of process parameters, a specific temperature and related flow field are established. If these fields are adequate to produce a sound weld, the process for existing system parameters is said to be optimized.

3 MODEL DESCRIPTION

The Finite Element (FE) model for FSSW plunge phase presented in this paper has been developed using commercial software ABAQUS/Explicit®. A 3-dimensional, transient, fully coupled thermal-stress analysis was performed to obtain thermo-mechanical responses of the workpiece.

The pre-processing involved the layout for the geometry of the parts, meshing, material and interaction assignments as well as initial and boundary conditions. Mesh adaptivity features of the software package was deployed by ALE formulations. The FSSW process was simulated by the model in multiple steps to allow mesh remapping between each step to control the mesh distortion and to ensure the quality of results.

The assembly of the model consisted of two parts; the workpiece and tool, as shown in Figure 4. The geometric dimensions are given in Figure 5. Two sheets of 3 mm thickness are modelled as one single sheet, 6 mm thick and 30 mm in diameter. This piece is taken into account for modelling.

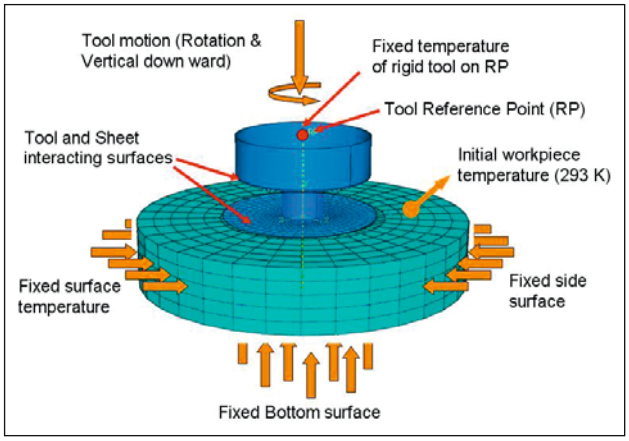

Figure 4 – Model assembly; rigid tool and workpiece along with the initial and boundary conditions

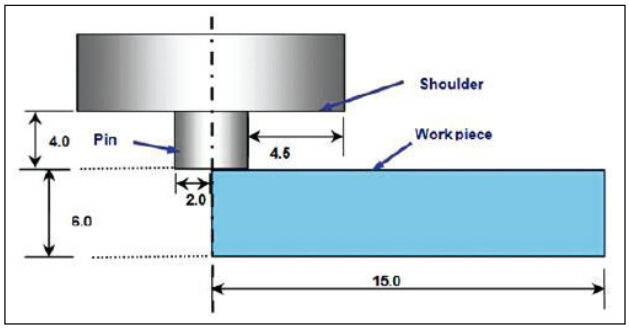

Figure 5 – Schematic details of model components i.e. tool and workpiece

Temperature and strain rate dependant Johnson-Cook (JC) material model for AA6082-T6 was assigned to the workpiece. The constitutive equation of this model and details of the material parameters used in this study are described in subsequent section. Other thermal and mechanical properties for AA 6082-T6 used in this study are given in Table 1 [21].

The tool is modelled as an analytical rigid body with adiabatic interfacial surface conditions, i.e. no heat flow across the interface of the tool could take place. The mesh of the workpiece consists of element type C3D8RT with reduced integration and hourglass control. This element type based upon explicit formulation for dynamic, fully coupled thermo-mechanical analysis is supported with Arbitrary Lagrangian Eulerian (ALE) mesh adaptivity.

Table 1 — Mechanical & thermal properties of AA6082-T6 used [21]

Temp. (K)	Young's Modulus (MPa)	Conductivity (W/m.K)	Specific heat capacity (J/kg.K)
293	7.50E+4	215	885
373	6.90E+4	212	915
473	5.60E+4	215	952
573	4.00E+4	216	992
673	2.60E+4	208	1 032
773	1.80E+4	202	1 073
853	-	196	1 113

This ALE formulation is employed in order to smooth the mesh while large deformations are taking place, particularly at tool-workpiece interface. The term ALE implies a broad range of analysis approaches, from purely Lagrangian analysis, in which the node motion corresponds to material motion, to purely Eulerian analysis, in which the nodes remain fixed in space and material "flows" through the elements. Typically ALE analyses use an approach between these two extremes [22, 23].

For calculation of heat generation during this study, the Coulomb's frictional heat generation model is employed using assessed coefficient of friction μ by the inverse approach [24, 25]. Due to the extremely dynamic nature of the process the determination of this parameter, which itself is multivariable dependent, is quite challenging. For example its trends may change even at constant slide velocity during a short instance when the applied loads due to non-linearity of the process are varied, as shown in Figure 6 [24].

For the theoretical studies in FSW/FSSW and in other similar friction processes the effective values of coefficient of friction are assumed [25]. This is done by adjusting parameters, such difficult to determine, to the experimentally measurable variables, like temperature, etc., i.e. the so-called inverse or engineering approach is followed [24-26].

In this work, this inverse approach was employed and the effective values of μ were assessed by simple iterative runs of the solver. The best fit was achieved when after the polynomial rise; the drop in the friction coefficient trend was assumed to follow the yield strength trend with respect to temperature. This trend is given in Figure 7.

Since during the FSW/FSSW process, heating is accomplished by frictional heat input and by energy dissipated due to plastic deformation of the workpiece [2], in the model, not only heat input by the Coulomb's model but also by deformational heat input was incorporated. For the heat dissipated into the workpiece due to deformation 95 % thermal efficiency is used, as suggested in [25].

Here, it would be worth mentioning that, although these two modes of heat generation are incorporated separately in the model, from a mechanism stand point, it is still a topic of discussion whether deformational energy dissipated as heat may be considered as an independent source or as a result of frictional conditions at the tool–workpiece interface.

The initial condition for the temperature within the workpiece was set at room temperature of 293 K. The thermal portion of the coupled analysis required thermal boundary conditions or loads on the rigid tool for the estimation of capacitance matrix, so the tool reference point (RP) was constrained to have a fixed temperature of 300 K. The overall applied boundary conditions are schematically shown in Figure 4. The rotational and plunge motion of the tool were incorporated as boundary conditions.

The numerical calculations were set to take place in multiple steps to incorporate mesh remapping between the steps and to ease out the mesh distortions from the previous step for the next one. Moreover, to enhance the computational efficiency of the simulation, mass scaling was also applied for mechanical module of the coupled thermal stress analysis. These topics are described in the next sections.

3.1 Numerical formulation

The FSW process involves coupled thermo-elasto-plastic response of the tool–workpiece system, in which the material model and the non-linear temperature dependent transient heat transfer response produce both temperature distribution and plastic deformations [3, 5]. To capture the thermo-mechanical response under the given system and process parameters, coupled temperature and displacement numerical formulations are used along with the heat generation factor.

The frictional heat generation formulation involves calculation of heat flux at the interface elements of the contacting parts (tool and workpiece) and this flux is applied as thermal load to the volume elements of each part. Thermal distribution to each surface may be given as in Equations (1) and (2) [22].

$$q_{(tool)} = q_k + q_r - f_{(tool)} q_g \quad (1)$$

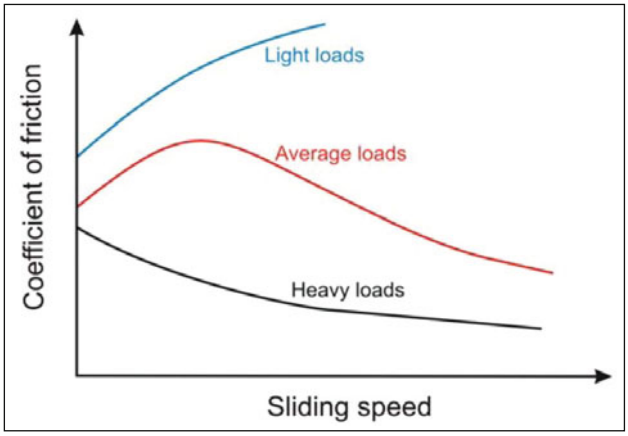

Figure 6 – Variation of friction coefficient with sliding speed and normal loads [24]

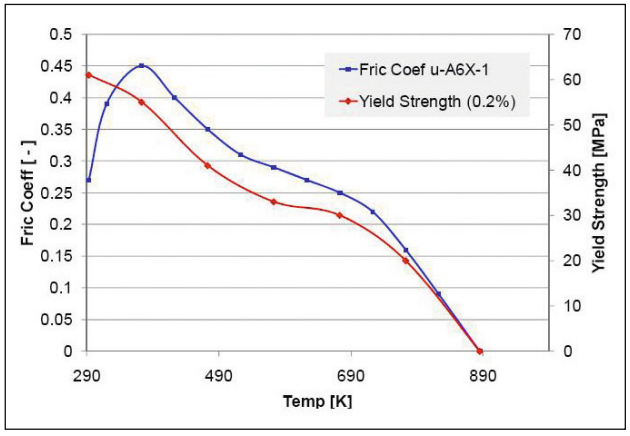

Figure 7 – Trends of assumed friction coefficient with respect to temperature

$$q_{(wp)} = -q_k - q_r - f_{(wp)}q_g \quad (2)$$

where

$q_{(tool)}$ = Thermal load as heat flux to the tool; [W.m^{-2}],

$q_{(wp)}$ = Thermal load as heat flux to the workpiece; [W.m^{-2}],

q_g = heat flux generated by the interface element due to friction; [W.m^{-2}],

q_k = heat flux due to conduction; [W.m^{-2}], and

q_r = heat flux due to radiation; [W.m^{-2}]

$f_{(tool}$, $f_{(wp)}$ = fraction of total generated heat (q_g) into tool and workpiece surface respectively; [-], such that $f_{(tool} + f_{(wp)} = 1$

For the current model, no heat flow occurs to the tool since the tool was defined as a rigid body with adiabatic conditions.

The heat flux generated at the interface elements due to friction may be given as in Equation (3).

$$q_g = \eta\tau\dot{s} = \eta\tau\frac{\Delta s}{\Delta t} \quad (3)$$

where

τ = frictional stress; [Pa],

$\dot{s}$ = slip rate; [m.s^{-1}],

Δs = slip increment; [m],

Δt = incremental time; [s], and

η = fraction of frictional work converted to heat; [-]

The frictional stress depends on the contact pressure, friction coefficient and temperature at the interface. Their relationship may be given as in Equation (4).

$$\tau = \mu(T).P(T) \quad (4)$$

where

μ = coefficient of friction; [-],

P = contact pressure; [Pa] and

T = temperature; [K]

The heat dissipated due to deformation is calculated as:

$$q_d = \alpha.\sigma.\dot{\varepsilon} \quad (5)$$

where

α = fraction of deformational energy dissipated as heat; [-],

σ = stress; [Pa] and

$\dot{\varepsilon}$ = strain rate; [s^{-1}]

The heat flux due to conduction is assumed to be:

$$q_k = k(h, p, T)(T_1 - T_2) = k(h, p, \bar{T})\Delta T \quad (6)$$

where

h = over-closure; [m] (penetration of master surface or nodes into the mesh of slave),

p = contact pressure; [Pa],

T_1, T_2 = temperatures of contact side 1 and side 2 respectively; [K],

$\bar{T} = \frac{1}{2}(T_1 + T_2)$ = average temperature at point contact; [K], and

$k(h, p, \bar{T})$ = heat transfer coefficient;

To incorporate hardening due to plastic deformation as a function of applied temperature, Johnson Cook material model, mathematically given in Equation (7), is extensively used for extrusion, forging and impact analysis, etc. [18]. It is also used in the reported theoretical works for the FSW/FSSW process e.g. [5, 18].

$$\bar{\sigma} = \left[A + B\left(\bar{\dot{\varepsilon}}^{pl}\right)^n\right]\left\{1 + C\ln\left(\frac{\bar{\dot{\varepsilon}}^{pl}}{\dot{\varepsilon}_\circ}\right)\right\}\left(1 - \hat{\theta}^m\right) \quad (7)$$

where

$\bar{\sigma}$ = effective yield strength; [Pa]

$\bar{\dot{\varepsilon}}^{pl}$ = equivalent plastic strain rate [s^{-1}]

$\dot{\varepsilon}_o$ = normalizing strain rate; [s^{-1}]

A, B, C, m, n = material parameters (given in Table 2)

$\hat{\theta}$ = non-dimensional temperature; [-], which is given as:

$$\hat{\theta} = \begin{cases} 0 & |\ \theta < \theta_{ref} \\ (\theta - \theta_{ref})\,/\,(\theta_{melt} - \theta_{ref}) & |\ \theta_{ref} \le \theta \le \theta_{melt} \\ 1 & |\ \theta > \theta_{melt} \end{cases} \quad (8)$$

where

θ = current temperature; [K]

θ_{ref} = reference temperature; [K]

θ_{melt} = melting temperature; [K]

The material parameters and the reference and melting temperatures used in this study are given in Table 2 [27].

3.2 Mesh distortion and its control

By employing the ALE formulation, large deformations may be simulated by re-meshing. It may be noted here that re-meshing by ALE does not imply the change in element density for ABAQUS/Explicit based models. The main point is to control the distortion of the elements by improving the aspect ratio of the distorted elements. This is done by the inter-step convection of results at the integration point and re-adjustment of nodal positions as close as possible to the original coordinates.

The effect of ALE on mesh distortion control is shown in Figure 8, for a 2-D simple mechanical model. When, between step-1 and step-2, ALE is employed, the

Table 2 – Johnson Cook parameters used for AA6082-T6 [27]

Parameters	A	B	n	C	M	θ^r_{ref}	θ^r_{melt}
Units	[MPa]	[MPa]	[-]	[-]	[-]	[K]	[K]
Value	428.5	327.7	1.008	0.00747	1.31	293	853

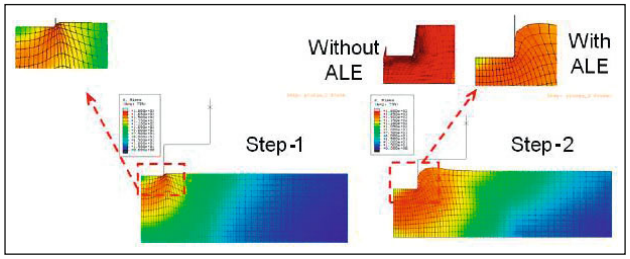

a) Step-1 b) Step-2

Figure 8 – Effect of ALE application between step-1 and step-2

results for step-2 remain stable, whereas, in absence of ALE, the solution is unstable and solver is excited due to distortion error.

The other approach to avoid this error could be to a use pure Eulerian mesh. As compared to pure Eulerian formulations, the advantage in using ALE formulation is that in ALE approach, the 'free' surfaces have Lagrange properties in the normal direction, such that surface tracking and partially filled elements are avoided. The position of the surface of the domain is found directly by solving the governing equation and no iterations are required [18, 22].

3.3 Computational time and mass scaling

In the ABAQUS/Explicit solver which is used for developing this thermal-stress coupled model, thermal and mechanical time increment limits may be given as Equations (9) and (10) [22]:

$$\Delta t = \frac{L_{\min}^2}{2\alpha} \tag{9}$$

where

L_{min} = smallest element dimension in the mesh; [m]

α = thermal diffusivity of the material; [$m^2.s^{-1}$]

$$\Delta t = \frac{L_{\min}}{c_d} \tag{10}$$

where

L_{min} = smallest element dimension in the mesh; [m]

c_d = dilatational wave speed; [$m.s^{-1}$], which can be expressed in terms of Lame's constants.

$$c_d = \left(\frac{\left(\frac{Ev}{(1+\nu)(1-2\nu)} + \frac{E}{(1+\nu)} \right)}{\rho} \right)^{\frac{1}{2}} \tag{11}$$

where

E = Modulus of elasticity; [Pa]

ν = Poisson's ratio; [-]

ρ = density; [$kg.m^{-3}$]

In the coupled thermal stress calculation the mechanical response will govern the stability limit. The stability criterion in mechanical response makes the increment size too small as the element dimensions are decreased. Hence computational time increases tremendously. Therefore use of mass scaling may be opted to decrease the calculation time.

The mass scale function scales the mass by applied factor, e.g. f, which alters the density and hence the inertia of the system. This slows down the dilatational wave or p-wave propagation speed, Equation (11), and reduces the calculation time, Equation (10). The use of mass scaling is equivalent to increasing the load rate by a factor of $(f)^{1/2}$, as per Equation (11). Caution should be taken as the use of mass scaling typically increases the simulated contact forces, which in turn could change the contact condition and the heat generation rate [18, 22].

4 EXPERIMENTAL SETUP

The friction stir spot welds were produced at the friction stir lab of Graz University of Technology using the MTS I-Stir BR4, Figure 9. This is an FSW portal machine with a tool rotational speed of up to 3 200 rpm, a maximum downward force of 35 kN and maximum spindle torque of 180 Nm. The machine is equipped with sensitive pressure actuated feedback instrumentation for forge force, position controls and torque outputs. With these instrumental accessories, online measurement of forge force response for each weld was obtained.

For this study the spot welds were made by using tools with different geometries but the same material (tool steel-H13). Geometries of the tools are shown in Figure 10.

Experiments with tool (a) are designated as Exp-set-1 and those with tool (b) as Exp-set-2. Exp-set-1, employing tool (a); with shorter pin, was used for thermal observations and Exp-set-2, employing tool (b); with longer pin, was used for thermo-mechanical response i.e. forge force. Process parameters in both sets are summarized in Tables 3 and 4.

Figure 9 – MTS stir-B4 research purpose FSW machine at IWS – TU Graz

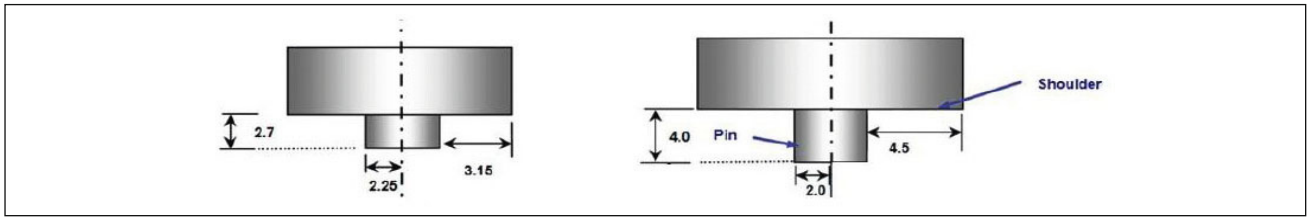

a) Tool (a)corresponding to Exp-set-1 **b) Tool (b)corresponding to Exp-set-2**

Figure 10 – Geometries of tools (a) and (b)

Table 3 – Process parameters in Exp-set-1 using tool (a)

Parameters / Trials	Rotational speed	Plunge rate	Dwell time
	RPM	mm/min	sec
Trial-1	1 400	~11.3	0
Trial-2	1 400	~11.3	1
Trial-3	1 400	~11.3	3

Table 4 – Process parameters in Exp-set-2 using tool (b)

Parameters / Trials	Rotational speed	Plunge rate	Dwell time
	RPM	mm/min	sec
Trial-1	800	12	0
Trial-2	1 200	12	0
Trial-3	1 600	12	0
Trial-4	2 000	12	0
Trial-5	800	60	0
Trial-6	800	72	0

For simulation, both the tools were with straight cylindrical pin without any threads and also with a flat shoulder which was without any features upon its surface. How-ever the tool used for thermal studies during the experiments i.e. tool (a) shown in Figure 10, had right threaded helix shoulder and right threaded pin features. The details of these features are shown in Figure 11 [21].

For thermal history measurements K-Type thermocouples were used. Temperature measurements were made just outside the tool-shoulder region in the workpiece shown schematically in Figure 12 a) and inter thermocouple locations are shown in Figure 12 b) [21]. Two

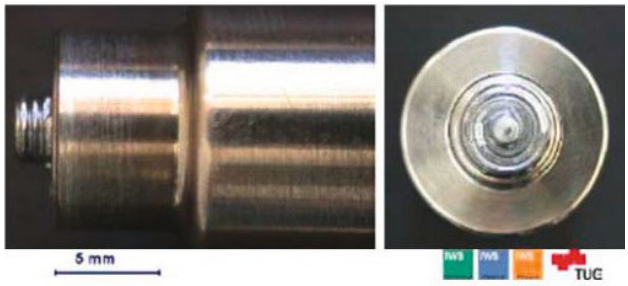

Figure 11 – Details of shoulder spiral and pin threads in "Tool (a)" [21]

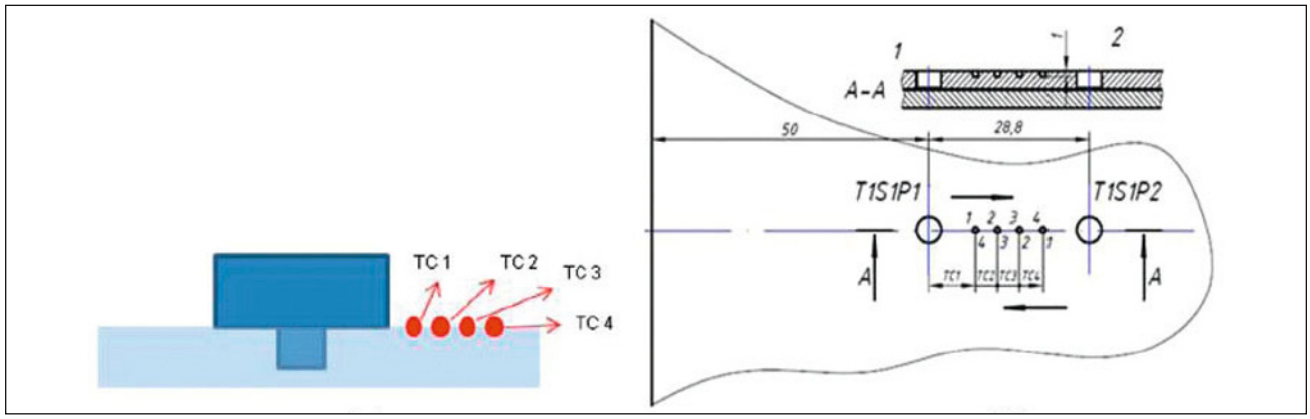

a) Schematic of thermocouple locations at region outside the tool-shoulder **b) Inter-spot dimensions with thermocouples in between**

Figure 12 [21]

Figure 13 – Thermocouples physical locations between two spots [21]

spots were at least 25 mm apart to keep a safe distance for thermal and deformational influences on each other and a similar approach was followed from the edges of the workpiece sheets. Physical location of thermocouples between the spots is shown in Figure 13 [21]. The measured forge force as well as temperature histories were used for model validation. A single sheet of 6 mm AA 6082-T6 was used during the experiments, for verifications of predicted results by computational study.

5 RESULTS AND DISCUSSION

For thermo-mechanical studies during FSSW, this work concentrates on the workpiece response to two important process parameters i.e. the rotational speed and the plunge rate of the tool. As an initial reference for the theoretical study, the experimental observations were made for the effect of tool rotational speed during exp-set-2.

The first notable effect was that an inverse relationship between the rotational speed and the size of the stir zone (SZ) was observed, as shown in the macrograph in Figure 14 [6].

The size of the stir zone at different rotational speeds is graphically presented in Figure 15 [6]. The radial reference “r (mm)” for SZ size, i.e. zero in this graph, is the centre of the weld and thickness reference “h (mm)” is the top surface of the workpiece. It may be clear from this figure that when the rotational speed was increased from 800 RPM to 2 000 RPM (Figures 14 and 15), by keeping the plunge rate constant, the size of SZ was reduced.

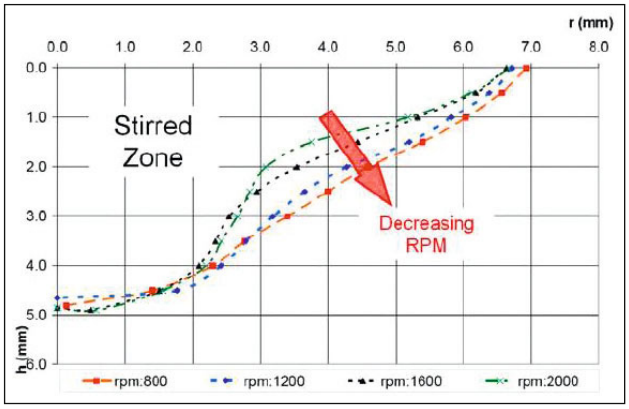

Figure 15 – Effect of rotational speed on the SZ size [6]

Further study for effect of the tool rotational speed on the forge force was made using the machine output data. Decrease in the forge force by increasing the rotational speed was observed as shown in Figure 16 [6].

The similarity in the trends of the SZ size and the forge force with respect to the rotational speed may be explained by the simplified conceptual mechanism approach that an increase in rotational speed increases the energy input rate, which leads to the formation of a relatively thinner but softer shear layer adjacent to the tool workpiece interface, as compared to the one at the lower rotational speeds. Within this shear layer at increased energy input rate, the drop in strength may reach a level that stress transmission to the next “layer-volume” of workpiece is reduced.

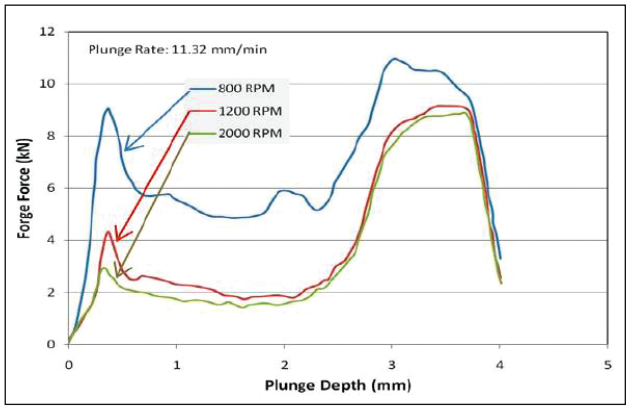

Figure 16 – Experimental output of forge force versus time at different rotational speeds [6]

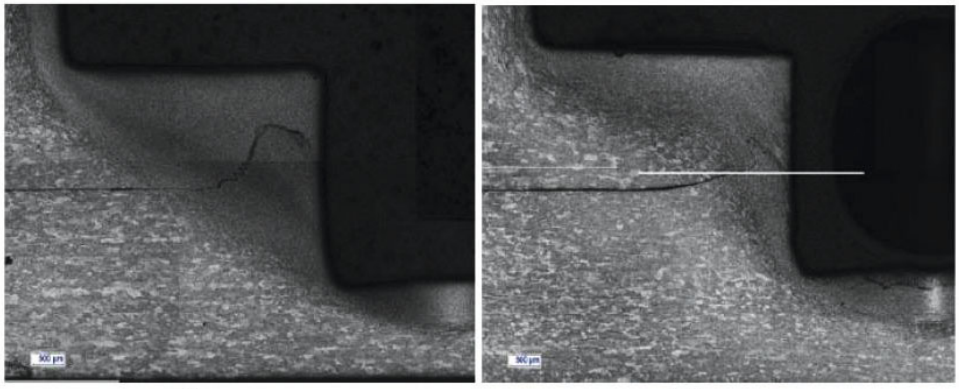

a) 800 RPM **b) 2 000 RPM**

Figure 14 – Macrographs showing different sizes of SZ [6]

From experimental results shown in Figure 16, a transient behaviour may be observed in forge force values generating a peak. This transient behaviour of initial rise of forge force to local maxima and then its drop may be explained by the conceptual mechanism flow chart. At the initial stage of plunge, the work hardening may continuously increase the yield stress of the material and hence the resistance to tool vertical motion. This may account for the initial rise of forge force during the plunge.

After certain plunge depth, a reduction in flow stress (material softening) due to a rise in temperature i.e. thermal softening of the material may be the reason for the forge force drop. Moreover the rise in temperature may also result in the dissolution of second phase particles present due to T6 treatment in this age hardenable aluminium alloy and hence contribute to material softening.

The forge force results from the theoretical investigation are shown in Figure 17. Effects of rotational speed on the forge force are also observed in these results i.e. lowering of forge force curve with increase in RPM. But in these results the initial phase of the plunge does not show the forge force increase and drop (transient response with local maxima) as in the experimental observations, Figure 16.

The apparent reason for this difference between the theoretical and the experimental results was assumed due to the difference in the plunge rates of the respective observations i.e. 72.0 mm/min for the computational study and 11.3 mm/min for the experimental one.

Therefore an experimental investigation was made to explore this assumption. As shown in Figure 18, the experimental investigation verified that by increasing the plunge rate to 72 mm/min resulted in no local maxima of the forge force i.e. similar to the one in the theoretical study. Here it may be worth mentioning that the other approach i.e. by adjusting the plunge rate in the theoretical study to the one in the experimental study was not carried out because enormous amount of computational time is required for the reported model at this slower plunge rate.

The reason for this behaviour may be that, at lower plunge rates, sufficient time is available for the thermal distribution by conduction in the surrounding workpiece volume, hence, a softened zone ahead of plunging tool may be developed. Thus the drop in forge force after initial rise may occur, whereas at faster plunge rates, due to lesser process time, the development of softened zone may not be adequate enough to drop the forge force.

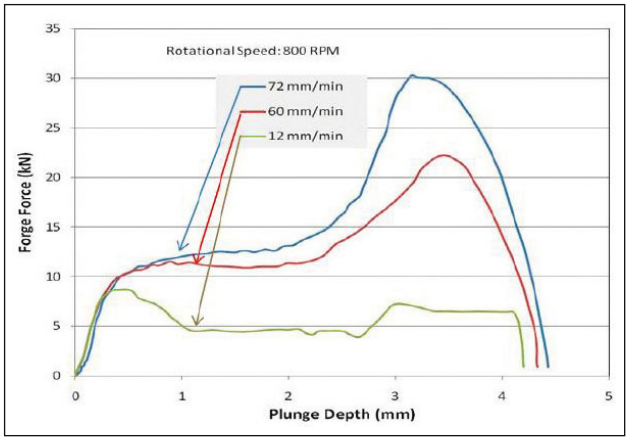

Figure 18 – Experimental results of plunge rate effects on the forge force

A theoretical study was also made for the effect of plunge rate on the forge force and the results are shown in Figure 19. These results also show the capability of this model to capture this non-linear effect. However, when these results are compared with those from the experiments, a difference of starting point for the forge force increase due to shoulder touch down is observed, Figure 20.

It should be noted that the pin length for both the experimental and the simulation studies was 4 mm. So, theoretically speaking, the rise in forge force should not be there before a 4 mm plunge depth of the tool. Whereas contrary to this, in experimental observations, these effects had started at a plunge depth of about 2.50-2.75 mm.

The reason for this may be the creation of flash, as shown in schematic Figure 1. The extent of this flash formation in the simulated results was much lower than those in the experimental. Hence, the difference in the slope and the starting point of rise in the forge force is due to shoulder touch down. This different flash forma-

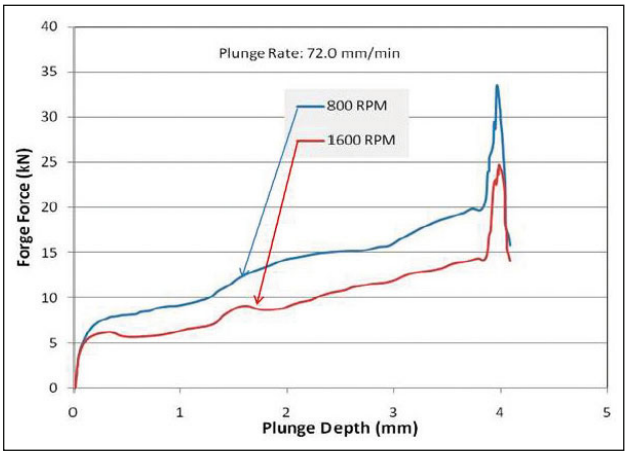

Figure 17 – Theoretical results of forge force for 800 and 1 600 RPM at 72 mm/min plunge rate

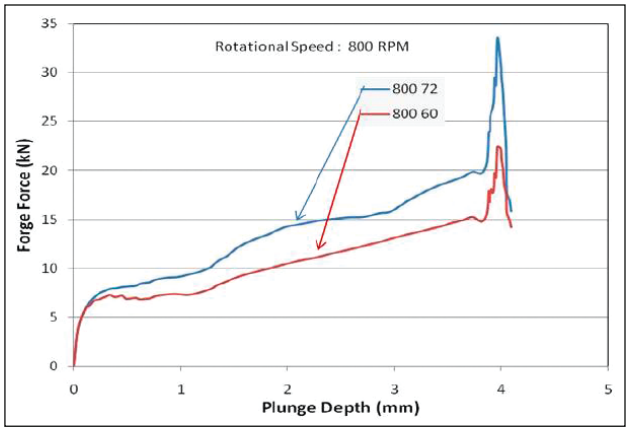

Figure 19 – Theoretical results of plunge rate effects on the forge force

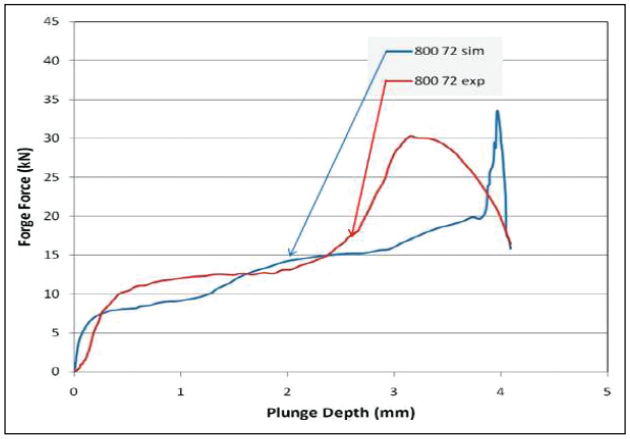

Figure 20 – Experimental and theoretical results of plunge rate effects on the forge force

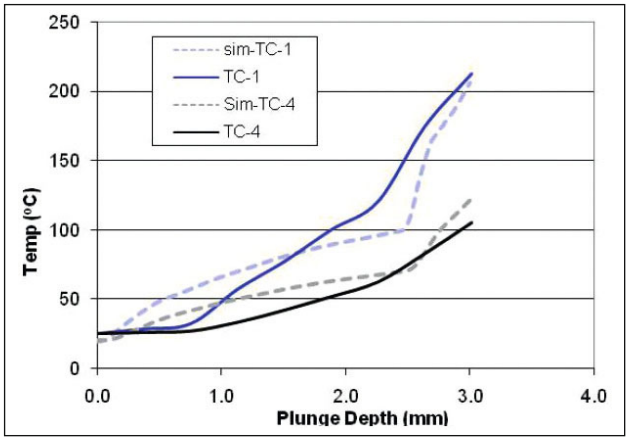

Figure 22 – Temperature history comparison between simulated and experimental results

tion in theoretical calculations and experimental observations may be due to approximation in the constitutive material model and/or to the parametric data used in the computational study.

Apart from this difference, overall trends of these simulation results may be termed in approximate agreement with those in the experimental, keeping the highly dynamic nature of the process in view.

For the validation of the model from thermal response point of view, results from exp-set-1 were used. From the computational study, where heat input was an additive balance of frictional and deformational heat inputs, the results were expected to be a little higher. For this expectation it may be stated that, since the tool is modelled as a rigid body and heat losses due to it are not included in the model, heat flow from tool – workpiece interface to the tool material reduces heat content within the workpiece in the physical process. Therefore this may be a main reason for relatively higher computed temperature values.

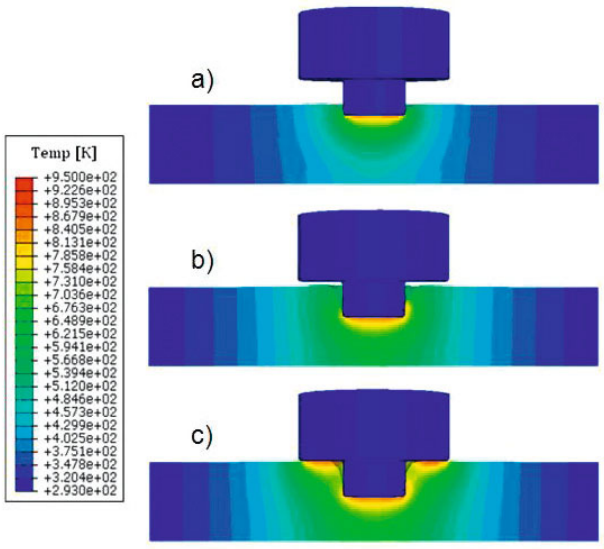

Figure 21 – Thermal profile as the tool plunges into the workpiece at 1 400 RPM (A); a) touchdown and initiation of plunge, b) pin penetration before the shoulder touchdown c) at shoulder touchdown

The thermal profile from computational results is shown in Figure 20 for different plunge depths. From this figure it may be clear that before the shoulder touchdown a maximum temperature occurred under the pin [Figures 21 a) and b)] and after the shoulder touchdown a maximum is found under the shoulder peripheral zone [Figure 21 c)]. The maximum temperature range is relatively higher as expected and discussed earlier.

The comparison of temperature history plots for two thermocouples placed just outside the shoulder periphery [as in Figure 12 a), at 11.2 mm and 15.15 mm from the weld centre respectively] in the workpiece is given in Figure 22. These trends show a reasonable agreement in general trends and a good agreement for the peak temperature values at these locations.

However, the difference in the slopes of these history plots, from the experiments and the simulation results, may also be attributed to the difference in the extent of flash formation during the pin penetration phase of the plunge since relatively higher heat input to the system would occur due to contact between the flash and the inner part of the tool-shoulder, prior to full touchdown of the shoulder area.

6 CONCLUSIONS AND OUTLOOK

– An experimental and computational thermo-mechanical study for FSSW or plunge phase of FSW was made to investigate the effects of process parameters i.e. tool rotational and plunge speeds on the thermal and forge force response of the workpiece i.e. AA 6082-T6.

– A conceptual mechanism frame work for the FSSW process was presented and its relevance with coupled thermal and stress behaviour during the FSSW process was discussed.

– For theoretical study, a physical-based, fully coupled thermo-mechanical model was developed to study the workpiece thermo-mechanical response and discussion was made in the light of proposed conceptual frame work for mechanisms of heat generation and interfacial conditions occurring during the process.

– As per experimental results of the SZ size and forge force analysis with respect to the rotational speed, an inverse relationship was observed between them.

– The developed model was able to predict this inverse relationship.

– Effects of plunge rate on the forge force were also studied experimentally as well as theoretically. Plunge rate showed a considerable influence on the resulting forces required to plunge the tool into the workpiece.

– Comparisons between theoretical and experimental results for forge force and thermal histories suggested the improvements in the material model, either by modification in the constitutive equation or by using experimental stress-strain data as function of temperature and strain rate, to predict the deformation in the near field of tool–workpiece interface, e.g. flash formation.

– Investigations for the relationship between energy input and its rate in term of rotational speed and plunge rate with the forge force, material deformation, heat generation and its distribution made the bases for mechanism understanding.

– More parametric studies are planned to enhance and strengthen the bases of proposed conceptual sequence to develop and further explore the mechanism of the process.

– Using the reported model as basic platform, incorporation of deformable tool and subsequent tool analysis e.g. tool geometry effects on thermo-mechanical and damage response etc. may be performed.

– The same model may be used to develop an integrated modelling approach e.g. by studying the microstructural evolution within workpiece during the FSSW process.

ACKNOWLEDGEMENTS

The financial support was given by Federal Ministry of Economy and Labour, Austria for this work on Friction Stir Welding related research through k-net JOIN project. S. Khosa acknowledges the scholarship for doctoral study from Higher Education Commission (HEC) of Pakistan.

REFERENCES

[1] Gerlich A., Avramovic-Cingara G., North T.H.: Stir zone microstructure and strain rate during Al 7075-T6 friction stir spot welding, Metallurgical and Materials Transactions A: Physical Metallurgy and Materials Science, 2006, vol. 37, no. 9, pp. 2773-2786.

[2] Mishra R.S., Ma Z.Y.: Friction Stir Welding and Processing, Materials Science and Engineering Reports, 2005, vol. 50, no. 1-2, pp. 1-78.

[3] Awang M., Mucino V., Feng Z., David S.: Thermo-mechanical modelling of FSSW Process, SAE International 2005-01-1251.

[4] Friction Stir Welding and Processing, R.S. Mishra, M.W. Mahoney, Editors, ASM Internationals, 2008, pp. 235-272.

[5] Mandal S., Rice J., Elmustafa A.: Experimental and numerical investigation of the plunge stage in friction stir welding, Journal of Materials Processing Technology, 2008, vol. 203, no. 1-3, pp. 411-419.

[6] Khosa S., Weinberger T., Enzinger N.: Material flow investigations during FSSW of Al 6082-T6 by FEA and experimental using different tool geometries, in University-Industry International Workshop (UIIW) at Nantes, France, June-2007.

[7] Colegrove P.A., Shercliff H.R.: 3-Dimensional CFD modelling of flow round a threaded FSW tool profile, Journal of Material Processing Technology, 2005, vol. 169, no. 2, pp. 320-327.

[8] Arora A., Zhang Z., De A., DebRoy T.: Strains and strain rates during friction stir welding, Scripta Materialia, 2009, vol. 61, no. 9, pp. 863-866.

[9] Su J.-Q., Nelson T.W., Mishra R., Mahoney M.: Microstructural Investigation of FSW 7050-T65 Aluminum, Acta Materialia, 2003, vol. 51, no. 3, pp. 713-729.

[10] Feng Z., Santella M.L., David S.A., Steel R.J., Packer S.M., Pan T., Kuo M., Bhatnagar R.S.: FSSW of Advanced High-Strength Steels – A Feasibility Study, SAE International 2005-01-1248, 2005.

[11] Connoly C.: Friction spot joining in aluminium car bodies, Industrial Robot: An International Journal, 2007, vol. 34, no.1, pp. 17-20.

[12] Figner G., Vallant R., Weinberger T., Schröttner H., Pašič H., Enzinger N.: Friction stir spot welds between aluminium and steel automotive sheets – Influence of welding parameters on mechanical properties and microstructure, Doc. IIW-1925-08 (ex-doc. SC-Auto-020r1-08), Welding in the World, 2009, vol. 53, no. 1/2, pp. R13-R23.

[13] Buffa G., Fratini L., Piacentini M.: On the influence of tool path in friction stir spot welding of aluminum alloys, Journal of Materials Processing Technology, 2008, vol. 208, no. 1-3, pp. 309-317.

[14] Badarinarayan H., Yang Q., Zhu S.: Effect of tool geometry on static strength of friction stir spot welded aluminium alloy, International Journal of Machine Tools and Manufacture, 2009, vol. 49, no. 2, pp. 142-148.

[15] Gerlich A., Su P., North T.: Tool penetration during friction stir spot welding of Al and Mg alloys, Journal of Materials Science, 2005, vol. 40, no. 24, pp. 6473-6481.

[16] Kakarla S.ST., Muci-Kuchler K.H., Arbegast W.J., Allen C.D.: Three-dimensional finite element model of friction stir spot welding process, Friction Stir Welding and Processing III, TMS, 2005, pp. 213-220.

[17] Guerdoux S., Miles M., Fourment L., Sorensen C.: Numerical simulation of the friction stir welding process using both Lagrangian and arbitrary Lagrangian Eularian formulations, Materials Processing and Design: Modeling, Simulation and Applications – NUMIFORM 2004 – Proceedings of the 8th International Conference on Numerical Methods in Industrial Forming Process, 2004, vol. 712, pp. 1259-1264.

[18] Schmidt H., Hattel J.: A local model for the thermo-mechanical conditions in friction stir welding, Modelling and Simulation in Materials Science and Engineering, 2005, vol. 13, no. 1, pp. 77-93.

[19] Schneider J., Beshears R., Nunes A.C. Jr.: Interfacial sticking and slipping in the friction stir welding process, Materials Science and Engineering A, 2006, vol. 435-436, pp. 297-304.

[20] Frigaard Ø., Grong Ø., Midling O.: A Process Model for friction stir welding of age hardening aluminium alloys, Metallurgical and Materials Transactions A, 2001, vol. 32, no. 5, pp. 1189-2000.

[21] Tasic P.: Predictions of temperature fields in work piece and tool during FSSW by using FEA, Diploma Thesis, IWS – TU Graz, 2006.

[22] DISIMULIA Abaqus User and Theory Manuals ver-6.7, 2008.

[23] Celigoj C., Außerlechner P.: A total ALE FE formulation for axisymmetric and torsional problems (including viscoplasticity, thermodynamic coupling and dynamics), International Journal for Numerical Methods in Engineering, 2006, vol. 70, no. 11, pp. 1324-1345.

[24] Maalekian M.: Friction welding – Critical assessment of literature, Science and Technology of Welding and Joining, 2007, vol. 12, no. 8, pp. 738-759.

[25] Maalekian M., Kozeschnik E., Brantner H.P., Cerjak H.: Inverse modelling and simulation of heat generation in friction welding, Mathematical modelling of weld phenomena 8, Cerjak H., Bhadeshia HKDB, Kozeschnik E., Editors, Verlag der Technischen Universität Graz, 2007, pp. 881-890.

[26] Chen C., Kovacevic R.: Thermomechanical modelling and force analysis of friction stir welding by finite element method, Proceedings of the Institution of Mechanical Engineers, Part C.: Journal of Mechanical Engineering Science, 2004, vol. 218, no. 5, pp. 509-519.

[27] Özel T., Zeren E.: Determination of work material flow stress and friction for FEA of machining using orthogonal cutting tests, Journal of Material Processing Technology, 2004, vol. 153-154, pp. 1019-1025.